ChemBioChem

Research Article
doi.org/10.1002/cbic.202400374

Chemistry Europe
European Chemical Societies Publishing

www.chembiochem.org

In-cell Catalysis by Tethered Organo–Osmium Complexes Generates Selectivity for Breast Cancer Cells

J. P. C. Coverdale,*[a, b] R. A. Bedford,[a] O. W. L. Carter,[b] S. Cao,[a] M. Wills,[b] and P. J. Sadler[b]

Anticancer agents that exhibit catalytic mechanisms of action offer a unique multi-targeting strategy to overcome drug resistance. Nonetheless, many in-cell catalysts in development are hindered by deactivation by endogenous nucleophiles. We have synthesised a highly potent, stable Os-based 16-electron half-sandwich ('piano stool') catalyst by introducing a permanent covalent tether between the arene and chelated diamine ligand. This catalyst exhibits antiproliferative activity comparable to the clinical drug cisplatin towards triple-negative breast cancer cells and can overcome tamoxifen resistance. Speciation experiments revealed Os to be almost exclusively albumin-bound in the extracellular medium, while cellular accumulation studies identified an energy-dependent, protein-mediated Os accumulation pathway, consistent with albumin-mediated uptake. Importantly, the tethered Os complex was active for in-cell transfer hydrogenation catalysis, initiated by co-administration of a non-toxic dose of sodium formate as a source of hydride, indicating that the Os catalyst is delivered to the cytosol of cancer cells intact. The mechanism of action involves the generation of reactive oxygen species (ROS), thus exploiting the inherent redox vulnerability of cancer cells, accompanied by selectivity for cancerous cells over non-tumorigenic cells.

Introduction

Catalysts lower activation energies and increase rates of reactions that would otherwise take place very slowly, if at all. In nature, enzymes (mainly proteins but also some ribonucleic acids) carry out biological transformations, and around a third are metalloenzymes.[1] These biological catalysts contain metal centres which play important roles in the overall mechanism of action. This has inspired the design of artificial enzymes and small molecule catalysts, and their possible use as anticancer agents has recently gained significant attention.[2] For example, Pd-mediated bioorthogonal activation of biochemically stable prodrugs has been described for the in vitro activation of precursors of 5-fluorouracil and gemcitabine to their active forms.[3] A similar strategy was employed for the in-cell catalytic activation of allyl carbamate protected amines to liberate deprotected doxorubicin using a Ru catalyst, achieving excellent bioorthogonal specificity and high substrate turnover, even in the presence of millimolar concentrations of thiols.[4] Another approach to achieve catalytic anticancer activity involves the catalytic oxidation of biomolecules; for which various half-sandwich organometallic catalysts of Rh, Ru, Ir, and Os have been described.[5] Those bearing iminopyridine or azopyridine bidentate ligands can achieve high potencies towards cancer cells, involving the catalytic generation of reactive oxygen species, and the catalytic oxidation of NADH to NAD^+.[6] Transition metal complexes can also catalyse transfer hydrogenation (reduction) reactions in the presence of a suitable hydride donor (commonly sodium formate).[2d,7] We have previously reported a new class of 16-electron Os arene complexes with the general formula [Os(arene)(diamine)], which can act as *in-cell* transfer hydrogenation (TH) catalysts,[8] and can achieve the enantioselective reduction of pyruvate to unnatural D-lactate in cancer cells (Figure 1, Os catalyst **4**).[9] To improve the efficiency of the catalytic activity in cells, a more comprehensive understanding of their distribution and their stability is required. Inductively coupled plasma mass spectrom-

[a] *Dr. J. P. C. Coverdale, R. A. Bedford, S. Cao*
School of Pharmacy, Institute of Clinical Sciences, College of Medical and Dental Sciences
University of Birmingham
Edgbaston, B15 2TT, UK
E-mail: j.p.coverdale@bham.ac.uk

[b] *Dr. J. P. C. Coverdale, Dr. O. W. L. Carter, Prof. M. Wills, Prof. P. J. Sadler*
Department of Chemistry
University of Warwick
Coventry, CV4 7AL, UK

Supporting information for this article is available on the WWW under https://doi.org/10.1002/cbic.202400374

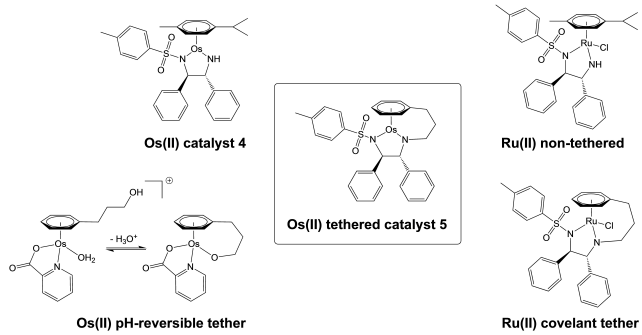

Figure 1. The structure of tethered Os(II) catalyst **5** studied in this work. Catalyst **4** and an 18-electron reversible-tethered Os(II) complex (left) have been previously reported to carry out the *in-cell* catalytic reduction of pyruvate to lactate.[9] Structurally similar Ru(II) *N*-tosyl–diphenylethylenediamine (TsDPEN) tethered and non-tethered complexes (right) are known to be active for transfer hydrogenation catalysis.[7]

etry (ICP-MS) and synchrotron X-ray fluorescence (XRF) elemental mapping experiments have identified an intracellular catalyst decomposition pathway involving loss of the diamine.[10]

Deactivation by loss of the arene has also been reported for Ru(II) analogues.[11] Such a loss of a chelated ligand would be expected to lead to loss of catalytic activity. Hence, structural modifications are being explored to design organo–metallic catalysts with improved stability in intracellular media. One strategy involves the inclusion of the active metal complex inside a protective protein scaffold, analogous to that of a natural metalloenzyme.[12] Nanoscale formulations have also been explored to improve tumor cell delivery and selectivity.[13] Alternatively, the metal complex could be stabilized by introduction of a covalent tether between the coordinated arene and the bidentate ligand, exploiting the chelate effect to improve complex stability. Complexes bearing a pH-sensitive reversible tether between the η^5 (Ir) or η^6 (Ru or Os) ligand and the monodentate coordination site have been shown to improve aqueous solution stability and can catalyse the *in-cell* reduction of pyruvate to lactate (Figure 1),[14] however, this reversible strategy does not address loss of the bidentate ligand. Ru(II) complexes bearing an irreversible (permanent) tether between the η^6-arene and the bidentate diamine ligand are well known (Figure 1, Ru TsDPEN catalysts).[15] Some examples of tethered catalysts have been explored for *in-cell* catalysis and were shown to modulate catalytically the intracellular NADH/NAD^+ ratio.[16] Non-tethered Os(II) TsDPEN catalysts are known,[8a,9] but arene–diamine-tethered Os(II) analogues of the aforementioned Ru(II) TsDPEN catalysts have not been synthesised previously (Figure 1).

Here, the first example of a covalently-tethered Os(II) complex is described, which can catalyse *in-cell* transfer hydrogenation reactions using formate as a H^- source. Its extracellular speciation was studied by LC-ICP-MS to investigate the stability of the complex, as well as interactions with serum proteins which might play a role in its cellular accumulation.

Results and Discussion

Initial efforts to synthesize a tethered Os(II) complex *via* an arene-exchange mechanism, as is routinely used for the synthesis of analogous Ru(II) complexes, proved ineffective.[17] Instead, tethered Os complexes were prepared from 3-(cyclohexadienyl)propan-1-ol, which was first converted to the corresponding triflate and then reacted with TsDPEN to afford tethered ligand **1** *via* a previously reported synthesis.[18] However, formation of the Os dimer, complex **3**, was unsuccessful using conventional reflux conditions. Nonetheless, dimer **3** was successfully obtained using microwave reaction conditions using $OsCl_3$ hydrate, as reported for similar metal–arene dimer complexes.[14c,19] Crucially, Os dimer **3** was prepared under acidic conditions to afford its amine salt and prevent premature coordination of the diamine ligand to the metal centre. Conversion of dimer **3** proceeded *via* a one-pot biphasic reaction in dichloromethane/water with potassium hydroxide gave complex **5** as a red crystalline solid, as similarly reported for the synthesis of untethered Os complex **4** from TsDPEN and $[OsCl_2(p\text{-cymene})]_2$ dimer (Scheme 1).[8a]

To understand how the inclusion of a 3-carbon tether would affect the geometry of the pseudo-planar 16-electron species, density functional theory calculations of complexes **4** (non-tethered) and **5** (tethered) were performed using Gaussian 16 (Figure 2).[20]

Molecular structures were generated using GaussView 6.0 based on previously reported crystallographic data for complex **4** and a structurally similar tethered ruthenium(II) TsDPEN complex (CCDC 273937).[8a,21] Geometries were optimized using the hybrid Perdew-Burke-Ernzerhof functional (PBE0) with the Lanl2DZ (including effective core potential for Os) and 6-31+G** (all other atoms) basis sets. Hessian analysis of the optimized structures showed no imaginary frequencies, confirming that the structures represented true energy minima. Os–N bond lengths were highly comparable between both structures (Os–N(Ts): 2.01 Å for both complexes; Os–N: 1.91 Å

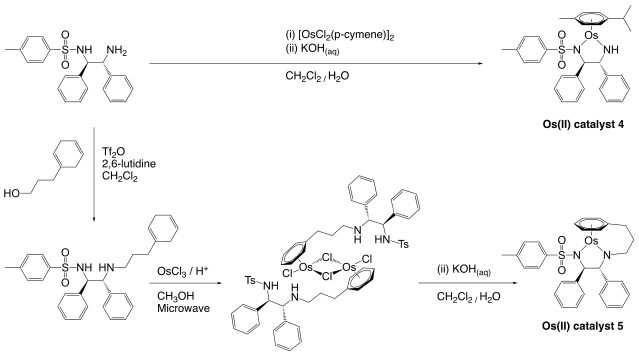

Scheme 1. Synthetic routes to either Os(II) arene complex **4** (non-tethered) or **5** (tethered) from chirally pure *N*-tosyl-1,2-diphenylethylenediamine (TsDPEN). Only (*R*,*R*)-configured enantiomers were prepared. Complex **4** was obtained *via* a one-pot biphasic reaction similar to a previous report.[8a] Complex **5** first requires conversion of TsDPEN to tethered ligand **1**, which is subsequently reacted with $OsCl_3$ hydrate under microwave conditions to afford tethered dimer complex **3**. Conversion of **3** to afford **5** proceeds *via* a similar one-pot biphasic reaction.

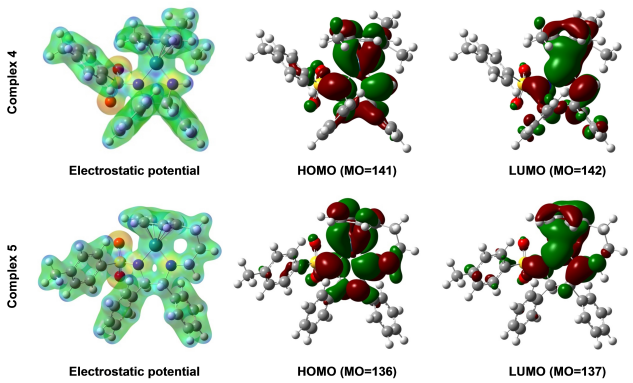

Figure 2. Density functional theory (DFT) calculations of the structure, electrostatic potential (mapped onto total electron density, −0.10 to +0.30), and HOMO/LUMO molecular orbitals for Os complexes **4** (non-tethered) and **5** (tethered) using the hybrid Perdew-Burke-Ernzerhof functional (PBE0) with the Lanl2DZ (including effective core potential for Os) and 6-31+G** (all other atoms) basis sets, using GaussView 6.0 and Gaussian 16.[20]

for complex **4**, 1.92 Å for complex **5**), and bond angles calculated in the carbon tether (ranging from 113.1–115.5°) are comparable to those determined experimentally in a structurally similar Ru(II) 3-carbon tethered complex (112.5–115.2°, CCDC 273937).[21] Electrostatic potential surfaces (EPS) showed similar charge distributions between complexes **4** and **5**, however, the calculated geometries revealed that the presence of an arene–diamine tether may hinder accessibility of the nitrogen atom for transfer hydrogenation. The critical importance of the N–H bond in TsDPEN-bearing catalysts for asymmetric transfer hydrogenation (ATH) is well known; similar Ru(II) tethered diamine–arene catalysts have been shown to maintain catalytic activity for ATH reactions while Ru(II) complexes containing two alkyl groups on the non-tosylated nitrogen atom are particularly poor catalysts.[22] Frontier molecular orbitals calculated for complexes **4** and **5** were also comparable (calculated HOMO-LUMO energy gaps of 4.13885 eV and 4.0289 eV respectively) emphasizing the marginal impact of tether introduction on the overall complex.

The catalytic activity of tethered Os(II) complex **5** was determined for transfer hydrogenation from formic acid to acetophenone, a common test substrate for transfer hydrogenation catalyst development (Table 1). Using a 0.5 mol% catalyst loading at 310 K, maximal turnover frequencies (TOF_{max}) were determined using time-dependent ^{1}H NMR spectroscopy by evaluating the formation of a new quartet resonance for 2-phenylethanol and a decrease in intensity of the singlet methyl resonance of acetophenone. For comparison, TOF_{max} values were also determined for non-tethered Os complex **4**. The measured TOF_{max} for tethered Os complex **5** ($20 \pm 1\ h^{-1}$) was significantly lower than that of non-tethered Os complex **4** ($63 \pm 2\ h^{-1}$, $>99\%$ conversion achieved within 24 h), which correlates with the steric hindrance predicted from DFT calculations. In contrast, the introduction of a covalent tether between the arene and diamine ligands in structurally similar Ru(II) arene complexes has been found to significantly enhance the rate of catalytic reduction of acetophenone.[15a] The origin of this difference between analogous Ru and Os tethered/non-tethered complexes remains unclear, but nonetheless highlights how the metal centre can have a significant impact on physicochemical properties.

With the knowledge that tethered Os catalyst **5** is active in an organic phase system (5:2 formic acid triethylamine azeotrope), the stability and speciation of **5** in aqueous media were investigated to assess its suitability for *in-cell* catalysis. Aqueous solutions of **5** were prepared using 5% v/v DMSO to aid solubility. Data obtained using UV-visible spectroscopy showed that complex **5** remained highly stable in cell culture medium (supplemented with 10% foetal calf serum) and human serum (10% v/v prepared in DPBS) in the presence of 5% v/v DMSO over a 24 h period (Supporting Information, Figure S2). Speciation was subsequently investigated by developing an offline LC-ICP-MS methodology, employing a TSKgel Q-STAT anion exchange column with an ammonium acetate/Tris binary mobile phase at physiological pH to quantify interactions between the Os catalyst and serum proteins (Figure 3). Extracellular speciation of **5** was determined in the presence of bovine serum albumin (BSA; 0.6 mM in DPBS) or foetal bovine serum to replicate cell culture experimental conditions, and additionally for comparison using human serum. Analysis of BSA incubated with complex **5** (Figure 3a) demonstrated Os to be almost exclusively BSA-bound ($t_R = 10$–13 min), while speciation measurements using FBS (Figure 3b) and human serum (Figure 3c) revealed the major Os-containing fractions (*ca.* 94–95% of total Os) to also coincide with the retention time of albumin, with the remaining Os (*ca.* 5–6%) recovered in the flow-through fractions ($t_R = 0$–3 min). Good Os recovery was achieved under all conditions (101–105%). Retention times for two abundant metalloproteins were also determined using single protein standards (human transferrin: $t_R = 6$–8 min, human albumin: $t_R = 10$–12 min, Figure 3d). Importantly, the high abundance of albumin in serum (35–50 $g \cdot L^{-1}$ physiological concentration) also means albumin is readily available to bind Os.[25] Although LC-ICP-MS studies detect only Os protein binding (and not that of complex **5** specifically), albumin has been shown to bind other metallodrugs, including two clinically trialed Ru(III) anticancer complexes, NAMI–A and KP1019/NKP1339, which retain biological activity after albumin binding.[26]

Antiproliferative activities ($IC_{50}/\mu M$) of Os complexes **4** and **5**, and the clinically used Pt drug, cisplatin were next determined towards seven human cell lines: A2780 ovarian cancer cells, A549 lung cancer cells, HCT-116 colorectal cancer cells, MCF7 breast cancer cells, MCF7–TAMR-1 tamoxifen-resistant breast cancer cells, MCF10-A non-tumorigenic breast cells, and MDA–MB-231 triple negative breast cancer (TNBC) cells (Table 2). Tethered Os complex **5** was more potent than non-tethered complex **4** and exhibited activity comparable to cisplatin towards breast cancer cell lines. The greater potency of the tethered complex compared to its non-tethered counterpart may be related to the greater structural stability offered by covalently linking the tosyl diamine and η^6-arene, afforded by the chelate effect. De-coordination of the 1,3-5-trimethylphenyl arene in structurally similar TH complexes has been described as being consistent with increased stability observed for of Ru tethered-arene catalysts.[11] Furthermore, we have previously shown that the release of a non-tethered diamine from Os coordination in the presence of endogenous thiols occurs inside cell lysosomes.[10] However, other factors such as uptake and distribution within the cell may also be important and warrant further investigation.

Table 1. Reduction of acetophenone, a model substrate for transfer hydrogenation catalysis, using either non-tethered Os 16-electron sulfonamide catalyst **4** or tethered Os 16-electron sulfonamide analogue **5** (0.5 mol%) in the presence of formic acid triethylamine azeotrope (source of hydride). Maximum turnover frequencies (TOF_{max}) were determined using time-dependent ^{1}H NMR spectroscopy (400 MHz, C_6D_6, 310 K).

Catalyst	S/C[a]	Temp/K	Tether	TOF_{max}/h^{-1}
4	200	310	No	63 ± 2
5	200	310	Yes	20 ± 1

[a] S/C substrate to catalyst ratio (S/C = 200 equivalent to 0.5 mol% catalyst loading).

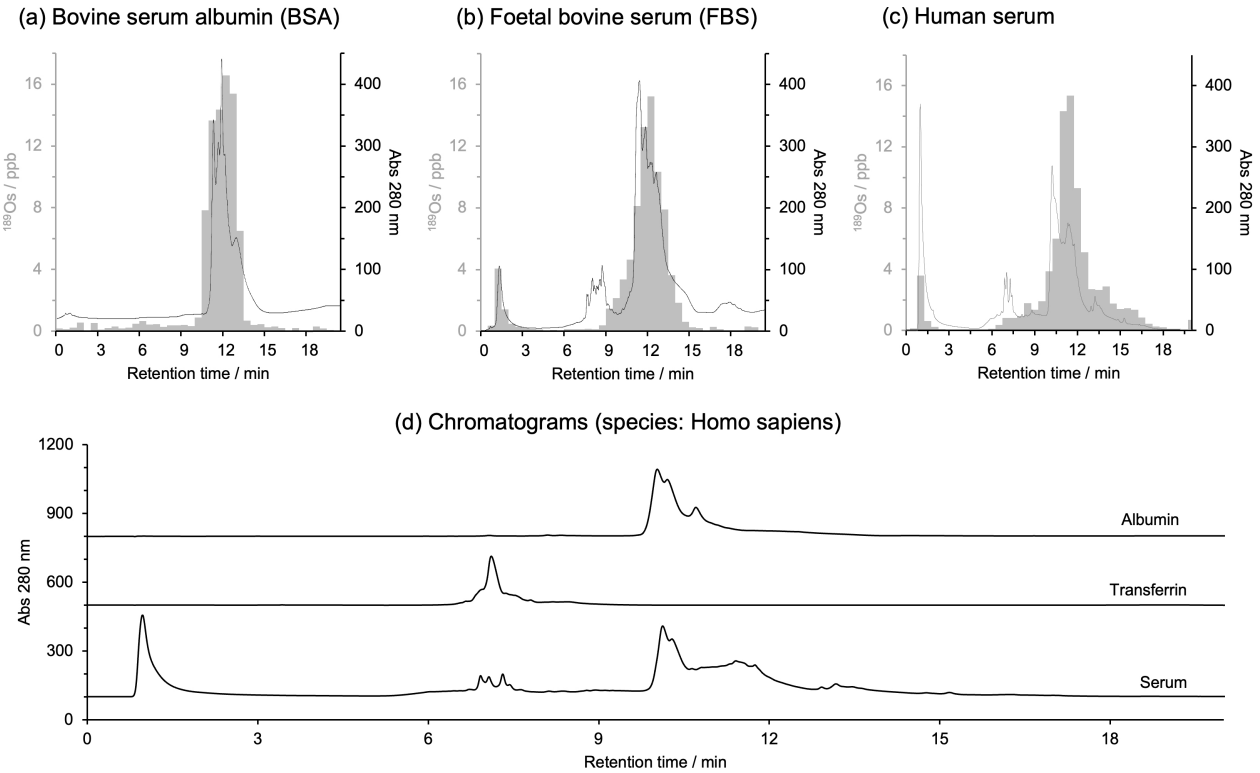

Figure 3. Extracellular speciation of tethered osmium catalyst **5** (15 μM, 310 K, 24 h), determined using offline LC-ICP-MS fitted with an anion exchange column (TSKgel Q-STAT). (a) Bovine serum albumin (BSA) incubated with **5** for 1 h. (b) Foetal bovine serum (FBS) incubated with **5** for 1 h. (c) Human serum incubated with **5** for 1 h. Recovery of Os by offline LC-ICP-MS speciation: BSA = 104.2%, FBS = 101.6%, human serum = 103.1%. (d) UV-visible chromatograms (absorbance at 280 nm, referenced to 360 nm) of single protein standards for human holo-transferrin (t_R = 6–8 min) and human serum albumin (t_R = 10–13 min) alongside human serum.

Table 2. Antiproliferative activities (IC_{50}/μM) determined for Os complexes **4** and **5**, cisplatin, and tamoxifen towards seven human cell lines: A2780 (ovarian carcinoma), A549 (lung carcinoma), HCT-116 (colorectal carcinoma), MCF7 (breast carcinoma; ER+, PR+ HER2−),[23] MCF7–TAMR-1 (tamoxifen-resistant breast carcinoma), MCF10-A (non-tumorigenic breast cells) and MDA–MB-231 (breast carcinoma; ER-, PR- HER2-).[23] Cells were treated for 24 h and allowed 72 h recovery time in drug-free medium. Cell viability was determined using the SRB assay.[24] N.D. = not determined.

		Antiproliferative activity/μM			
Cell line	Description	Complex **4**	Complex **5**	Cisplatin	Tamoxifen
A2780	Ovarian	15.5 ± 0.5	10.5 ± 0.1	1.2 ± 0.3	12.4 ± 0.1
A549	Lung	21.1 ± 0.3	14.1 ± 0.3	3.2 ± 0.1	13.5 ± 0.1
HCT-116	Colorectal	37 ± 1	36.4 ± 0.2	5.2 ± 0.3	19 ± 3
MCF7	Breast (ER+, PR+ HER2−)	11.0 ± 0.3	8.1 ± 0.2	6.6 ± 0.2	5.9 ± 0.4
MCF7–TAMR-1	Breast (tamoxifen-resistant)	N.D.	9 ± 1	6.0 ± 0.7	14.5 ± 0.1
MCF10-A	Breast (non-tumorigenic)	N.D.	30.9 ± 0.4	6 ± 1	25.0 ± 0.2
MDA–MB-231	Breast (ER-, PR- HER2-)	15 ± 1	9.1 ± 0.9	9.6 ± 0.4	12.9 ± 0.2

The activity of **5** was similar towards tamoxifen-resistant MCF7–TAMR-1 breast cancer cells compared to tamoxifen-sensitive MCF7 cells (P = 0.52), while a 2.4-fold activity decrease was observed for cells treated with tamoxifen (Table 2) confirming the MCF7–TAMR-1 resistance phenotype. Interestingly, **5** also displayed excellent activity towards MDA–MB-231 TNBC cells, with potency comparable to that of cisplatin (IC_{50} = 9.1 ± 0.9 μM for **5**, compared to 9.6 ± 0.4 μM for cisplatin, Table 2). TNBCs lack expression of oestrogen (ER), progesterone (PR), and human epidermal growth factor receptor 2 (HER2) receptors,[27] and are associated with a high incidence of recurrence, metastases, and poor clinical prognosis,[28] and are considered the most aggressive subtype of breast cancers.[27] Though platinum therapies are effective in neoadjuvant chemotherapy regimens toward TNBCs,[29] they are associated with increased hematological toxicity.[30] As such, the ability of **5** to overcome drug resistance and maintain activity towards MCF7–TAMR-1 tamoxifen-resistant cells and MDA–MB-231 TNBC cells is highly promising. Encouragingly, **5** was significantly also less toxic towards non-tumorigenic breast cells (MCF10-A, IC_{50} = 30.9 ± 0.4 μM) compared to breast cancer cells (MCF7, MCF7–TAMR-1, MDA–MB-231, IC_{50} 8.1–9.1 μM). This was

not the case for cisplatin, which exhibited similar potency towards cancerous and non-cancerous breast cells (6.6 ± 0.2 μM and 6 ± 1 μM toward MCF7 and MCF10-A cells, respectively).

The zebrafish embryo model has been shown to successfully and reliably predict drug toxicity in humans,[31] supported by correlations in cardiotoxicity, hepatotoxicity and nephrotoxicity between zebrafish and humans.[32] The genomes of zebrafish and humans are highly comparable,[33] with around 75% of human genes having at least one zebrafish orthologue.[34] Acute *in vivo* toxicities of complex **5** and cisplatin were determined according to OECD Test 236, where **5** was found to exhibit 9× less acute toxicity towards zebrafish embryos compared to cisplatin (Complex **5** LC_{50} = 5.2 ± 0.3 μM; cisplatin LC_{50} = 0.6 ± 0.2 μM), supporting its suitability for future therapeutic development.

Focusing on the specific application of tethered complex **5** in breast cancer cells, metal accumulation studies were carried out using MCF7 cells treated with **5** (fixed concentration equal to 1×IC_{50} = 8.1 μM) and Os quantification was achieved using ICP-MS analysis of acid-digested cell pellets. Time-dependent measurements (Figure 4a) revealed the maximal Os accumulation occurs 6 h after commencing exposure to complex **5**, with only ca. 66% of the maximum Os accumulated being present after 24 h exposure. Similar time-dependent accumulation profiles have been reported for non-tethered complex **4** and structurally similar Os azopyridine complexes in A2780 ovarian cancer cells, which also achieved maximal Os accumulation after 6 h.[9,36] Non-tethered complex **4** is less potent than tethered complex **5** (15.5 ± 0.5 μM vs. 10.5 μM ± 0.1 in A2780), and accordingly, Os accumulation in MCF7 cells after equipotent treatment was found to be *ca.* 2.5-fold greater for cells treated with **4** (complex **4**: 33 ± 2 fg·cell^{-1}, complex **5**: 13.1 ± 0.5 fg·cell^{-1}). In addition, to replicate the experimental conditions used during antiproliferative activity studies, cells were also exposed to complex **5** for 24 h and then further incubated for 72 h in Os-free medium ('recovery time'). After 72 h, over *ca.* 95% of the maximal Os accumulated (t = 6 h) was no longer present.

To explore the mechanism of cellular efflux, experiments were repeated in the presence of 20 μM verapamil (a selective inhibitor of the P-gp efflux transporter) in the recovery medium (Figure 4a, dashed line).[37] The presence of verapamil did increase the intracellular Os concentration ($P < 0.001$) relative to the verapamil-free control, yet the majority of Os was still exported after 72 h recovery. As such, the contribution of P-gp to the overall efflux of **5** is likely minor, which was also observed previously in A2780 cells using complex **4**.[9]

Cellular accumulation studies were repeated in MDA–MB-231 TNBC cells to investigate correlations between potency and accumulation in breast cancer cells. In agreement with the similar IC_{50} values determined for complex **5** in MCF7 (8.1 ± 0.2 μM) and MDA–MB-231 (9.1 ± 0.9 μM), cellular Os accumulation in TNBC cells (14.9 ± 0.8 fg·cell^{-1}) was remarkably comparable to that of MCF7 cells (13.1 ± 0.5 fg·cell^{-1}). This may indicate that there is a common mechanism of cellular accumulation, and perhaps also a similar *in-cell* mechanism of action.

To probe the mechanism of cellular uptake, Os accumulation was determined in MCF7 breast cancer cells treated with tethered complex **5** in the presence of various known uptake (influx) pathway inhibitors (Figure 4b).[35] Co-administration with

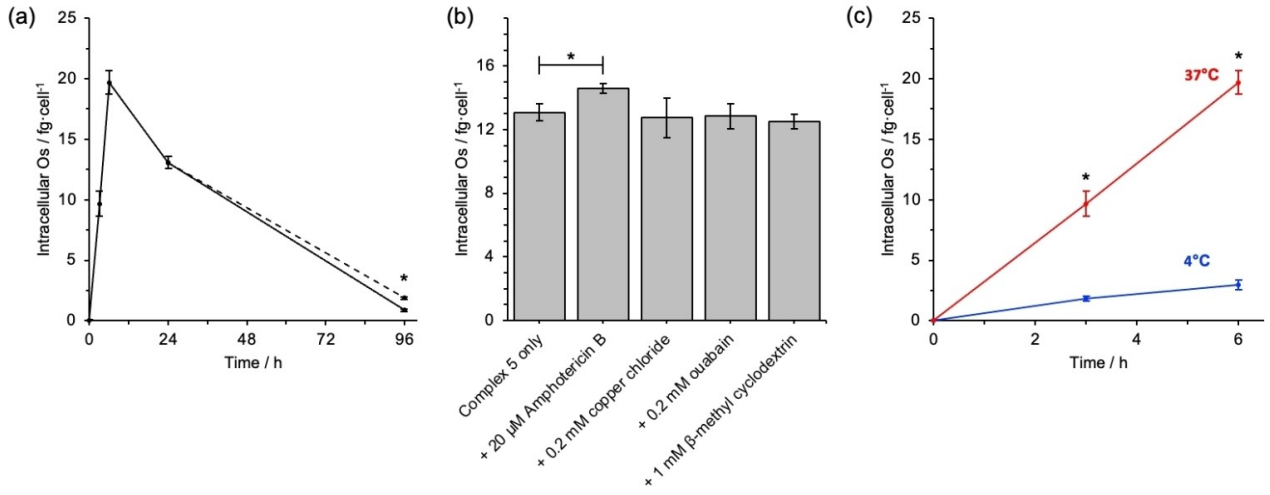

Figure 4. Cellular Os accumulation in MCF7 breast cancer cells treated with tethered complex **5** (1×IC_{50}). (a) Time-dependent Os accumulation: 0–24 h exposure to complex **5** followed by 72 h recovery time in Os-free medium. Solid line indicates complex **5** only, dashed line indicates recovery time (72 h) in the presence of 20 μM verapamil, a potent inhibitor of the P-gp efflux transporter. Os accumulation reaches a maximum concentration after 6 h exposure, after which time intracellular Os decreases. After 72 h recovery, > 95% of Os has been exported from cells. (b) Os accumulation (24 h) in cells treated with complex **5** in combination with: 20 μM amphotericin B (causes membrane disruption as a model for protein-mediated uptake), 0.2 mM Cu(II) chloride (competitive uptake *via* Ctr1), 0.2 mM ouabain (inhibitor of Na^+/K^+ pump to investigate the role of membrane potential), and 1 mM β-methyl cyclodextrin (inhibitor of caveolin-mediated endocytosis).[35] The accumulation of Os in cells treated with complex **5** is significantly increased by the presence of amphotericin B. (c) Temperature-dependent Os accumulation (3–6 h) experiments in cells treated with complex **5** reveal significantly lower accumulation at lower temperature, suggesting the contribution of energy-dependent (active-transport) cellular uptake mechanisms. Data shown are mean values with error bars representing ± 1 standard deviation. Full numerical and statistical data can be found in the Supporting Information. Statistical significances were determined using a two-tailed t-test assuming unequal sample variances (*$p < 0.05$).

non-toxic concentrations of Cu(II) chloride (0.2 mM, a competitive substrate for Ctr1 which is known to contribute to the uptake of Pt drugs), ouabain (0.2 mM, $Na+/K+$ pump inhibitor, to investigate the role of membrane potential in metallodrug uptake) and β-methyl cyclodextrin (1 mM, inhibitor of caveolin-mediated endocytosis) had no significant effect on the accumulation of Os after 24 h. However, co-administration of complex **5** with amphotericin B (20 μM), which causes membrane disruption as a model for protein-mediated uptake, was found to significantly increase the accumulation of Os, relative to cells administered with complex **5** alone ($P=0.0277$). Os accumulation determined at 277 K (Figure 4c) further highlighted the significant contribution of energy-dependent transport mechanisms to the accumulation of Os. In summary, extracellular speciation studies and intracellular accumulation measurements demonstrate that Os from complex **5** is almost exclusively albumin-bound in the extracellular environment and appears to be accumulated by cells *via* a protein-mediated, energy-dependent transport mechanism.

Many metal–arene complexes are known to perturb the cellular redox balance as part of a multi-targeting mechanism of action.[38] Since complex **5** was shown to be an active catalyst for transfer hydrogenation reactions in a chemical system, the qualitative level of reactive oxygen species (ROS) generated by complex **5** in cells was explored using fluorescence microscopy. After 24 h exposure to **5**, MCF7 cells were stained using 2′,7′-dichlorodihydrofluorescein diacetate (H_2–DCFDA), a membrane permeable non-fluorescent precursor which undergoes intracellular decarboxylation and is then oxidised by various intracellular reactive oxygen-based or reactive nitrogen-based species (ROS and RNS, respectively) to fluorescent DCF ($\lambda_{Ex/Em}=$ 485/530 nm).[39] The assay was validated using a known inducer of cellular ROS (50 μM Antimycin A, 30 min, Figure 5).[39b,40] DCF fluorescence was measured in cells treated with complex **5**, where increased fluorescence indicated significantly elevated ROS relative to the untreated control. This was also previously observed for non-tethered complex **4** in ovarian and breast cancer cells,[41] consequently identifying a commonality in the mechanism of action of Os(II) tosyl–diamine complexes. Given

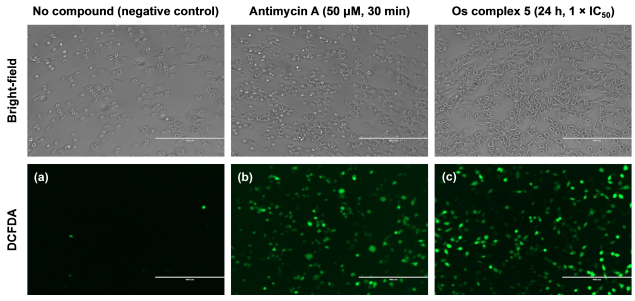

Figure 5. Detection of ROS in MCF7 breast cancer cells by fluorescence microscopy (10× magnification): (a) negative control (no test compound), (b) treated with Antimycin A (positive control, 50 μM, 30 min), (c) treated with tethered Os complex **5** ($1\times IC_{50}$, 8 μM, 24 h). Cells were stained using 2′,7′-dichlorodihydrofluorescein diacetate (H_2–DCFDA, 20 min in the dark), a membrane permeable indicator of intracellular ROS and were washed twice with DPBS prior to imaging to remove excess H_2–DCFDA. Cells were imaged using an EVOS FL fluorescence microscope fitted with a GFP filter cube ($\lambda_{Ex/Em}=$ 470/510 nm, exposure time 0.5 sec, intensity 50%).

the structural similarity between complexes **4** and **5**, this mechanistic commonality is perhaps unsurprising, but nonetheless encouraged the further exploration of complex **5** as a redox- modulating agent. This qualitative analysis of intracellular ROS illustrates that the generation of intracellular ROS is not hindered by the introduction of the covalent tether. Future studies should explore ROS generation in triple-negative MDA–MB-231 cells, though such a detailed mechanistic study goes beyond the scope of this work. Chemical catalysis using formic acid as a source of hydride (Table 1) demonstrated that complex **5** can catalyse TH reactions. Using the sodium salt of formic acid as a hydride donor, *in-cell* catalysis was studied by co-administration of a sub-lethal dose of **5** ($0.5\times IC_{50}$) alongside a non-toxic concentration of formate (0–2 mM) in MCF7 cells. In the absence of Os complex (Figure 6a), formate had no significant effect on cell survival, confirming that the co-factor is non-toxic in this concentration range. However, in the presence of tethered complex **5** (Figure 6c), cell survival significantly decreased with increasing formate concentration. The specific role of formate as a hydride donor in a TH mechanism was confirmed by substituting formate by acetate, which cannot donate hydride: in this case, there was no significant impact on cell survival irrespective of the presence or absence of complex **5** (Figures 6b and 6d). Importantly, accumulation of Os in cells is not affected by the presence of formate, demonstrating that the co-factor does not modulate cellular accumulation of complex **5**, thus the observed reduction in cell survival is likely attributable to an *in-cell* catalytic mechanism of action (Supporting Information Table S2).

Activity modulation experiments using sodium formate and sodium acetate were repeated in MDA–MB-231 (TNBC) cells (Figures 6e–h and Supporting Information), where the *in-cell* catalytic mechanism was conserved. Decreased cell viability was observed by increasing formate co-administration (Figure 6g), while no effect was observed in the presence of acetate (Figure 6h). In achieving *in-cell* catalysis in TNBC cells, which has also been observed with structurally related Os–arene catalysts,[14c] we demonstrate how this *in-cell* catalytic mechanism of action could be applied to treat cancers which currently have limited treatment options. Finally, activity modulation experiments using formate and acetate were repeated using MCF10-A non-tumorigenic cells (Figures 6i–l and Supporting Information) as a model of healthy cells. Similarly to previous observations using untethered Os catalyst **4** in a healthy ovarian cell model,[9] formate co-administration did not enhance the potency of complex **5** (Figure 6k). This critical finding highlights the potential of *in-cell* transfer hydrogenation to offer a unique approach to enhance selectivity for cancer cells over non-cancerous cells.

The successful delivery of an intact metallodrug is essential to achieve *in-cell* catalysis. The ability of complex **5** to facilitate *in-cell* catalysis in breast cancer cells (MCF7 and MDA-–MB-231) suggests that the extracellular albumin-bound Os species, which is accumulated in cells *via* a protein-mediated uptake mechanism, must result in the successful delivery of the intact active transfer hydrogenation catalyst **5** to cells. This is consistent with our previous work using a Br-containing

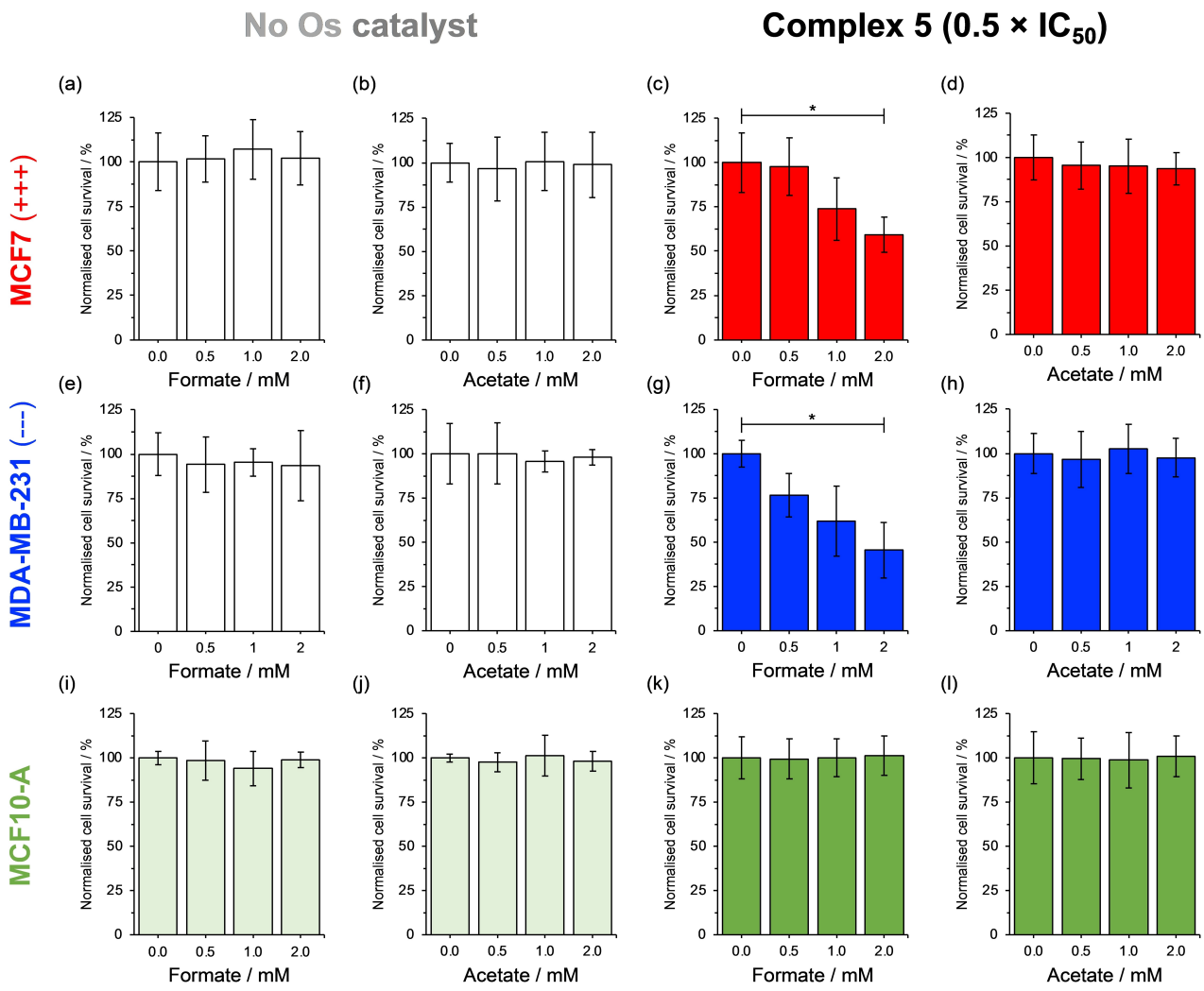

Figure 6. Activity modulation of complex **5** in MCF7 (breast cancer, a–d), MDA–MB-231 (TNBC breast cancer, e–h) and MCF10-A (non-tumorigenic breast, i–l) cells using non-toxic 0–2 mM concentrations of sodium formate (a, c, e, g, i, k) or sodium acetate (b, d, f, h, j, l). Cells were either treated with formate or acetate in the absence of complex **5** (a, b, e, f, i, j) or a sub-lethal concentration of complex **5** equal to 0.5×IC_{50} (c, d, g, h, k, l). Cell survival (%) was determined using the sulforhodamine B assay after 24 h exposure + 72 h recovery time in fresh culture medium. Data shown are mean values of three biological replicates with error bars representing ± 1 standard deviation. Full numerical and statistical data are found in the Supporting Information. Statistical significances were determined using a two-tailed t-test assuming unequal sample variances (*$p < 0.05$).

diamine analogue of non-tethered complex **4**, where X-ray fluorescence elemental mapping revealed the Br-containing diamine and Os to be co-localized in cells.[10]

Conclusions

Novel covalently-tethered organo–osmium TsDPEN catalyst **5** was synthesized using microwave radiation of a chlorido bridged Os dimer intermediate. Catalytic rates (TOF_{max}) measured for the transfer hydrogenation of acetophenone by tethered complex **5** were slower than for non-tethered Os complex **4**. However, tethered Os complex **5** was more potent towards cancer cells than its non-tethered analogue, in some instances achieving potency comparable to cisplatin. Extracellular speciation measurements revealed Os to be almost exclusively albumin-bound in human serum, in agreement with the protein-mediated, energy-dependent uptake pathway identified in cellular Os accumulation studies. The mechanism of action of complex **5** is likely to be multi-targeted, involving modulation of cellular redox balance (as evidenced by the generation of ROS inside cells) and an *in-cell* catalytic mechanism which was conserved in both triple-positive and triple-negative breast cancer cells. Importantly, we highlight that the catalytic mechanism generates selectivity for cancer cells over non-tumorigenic cells. Future work will involve characterizing the nature of the extracellular albumin–Os binding, further characterization of the specific albumin-mediated uptake pathway, and exploration of the intracellular Os speciation in relation to catalyst deactivation and detoxification.

Experimental Section

Synthesis of Tethered Ligand 1

Ligand **1** was prepared as previously reported.[21] To a cooled (0 °C) solution of 3-(1,4-cyclohexadien-1-yl)-1-propanol (553 mg, 4.0 mmol, 1.6 equiv.) and 2,6-lutidine (613 μL, 5.25 mmol, 2.10 equiv.) in anhydrous dichloromethane (20 mL) was added slowly a solution of trifluoromethane sulfonic anhydride (728 μL, 4.3 mmol, 1.7 equiv.) in anhydrous dichloromethane (10 mL). The reaction temperature was maintained at 0 °C for 30 min, followed by warming to ambient temperature for 1 h. After re-cooling to 0 °C, a solution of (*R*,*R*)-TsDPEN (915 mg, 2.5 mmol, 1.0 equiv.) and triethylamine (838 μL, 6.0 mmol, 2.4 equiv.) in anhydrous dichloromethane (20 mL) was added dropwise and stirred for 3 h. The resultant solution was diluted with additional dichloromethane (50 mL) and washed with saturated aqueous sodium hydrogen carbonate (3×100 mL), water (2×100 mL) and brine (1×100 mL). The organic phase was dried over magnesium sulphate and concentrated to afford an amber oil. The oil was recrystallized in hot ethanol and filtered to obtain **1** as a white amorphous solid, which was washed with cold ethanol and diethyl ether (968.4 mg, 2.00 mmol, 80%).^{1}H NMR (400 MHz, $(CD_3)_2SO$, 25 °C, TMS): δ = 7.37 (d, ArH, ^3J(H,H) = 8.1 Hz, 2H), 7.13 (m, ArH, 3H), 7.04 (m, ArH, 5H), 6.95 (m, ArH, 2H), 6.91 (m, ArH, 2H), 6.28 (*br* s, NH, 1H), 5.69 (m, CH, 2H), 5.31 (s, CH, 1H), 4.24 (d, CH, ^3J(H,H) = 7.8 Hz, 1H), 3.60 (d, CH, ^3J(H,H) = 7.8 Hz, 1H), 2.64 (m, CH_2, 2H), 2.52 (m, CH_2, 2H), 2.34 (s, CH_3, 3H), 1.88 (m, CH_2, 2H), 1.51 (m, CH_2, 4H). ESI-MS: *m/z* = 487.2.

Synthesis of Non-Tethered $[OsCl_2(p\text{-Cymene})]_2$ Dimer 2

Os dimer **2** was prepared as previously reported.[19] To a solution of Os(III) chloride trihydrate (1.00 g, 2.8 mmol, 2 equiv.) in methanol (10 mL) was added α-phellandrene (3.80 g, 28 mmol, 20 equiv.). The solution was subject to microwave-assisted reaction (CEM Discovery-SP microwave, 150 W, 250 psi, 413 K, 10 min) and then cooled to ambient temperature. An orange crystalline precipitate was obtained by addition of n-pentane (3×10 mL) and agitation, which was collected by filtration and washed with n-pentane and diethyl ether (863 mg, 1.11 mmol, 79%). Characterisation data matched those previously reported for the $[OsCl_2(p\text{-cymene})]_2$ dimer.[8a]

Synthesis of Pre-Tether Osmium Dimer 3

To a solution of Os(III) chloride trihydrate (175 mg, 0.50 mmol, 1 equiv.) in methanol (5 mL) was added tethered ligand **1** (292 mg, 0.60 mmol, 1.2 equiv.) and hydrochloric acid (75 μL 37% HCl, 0.90 mmol, 1.8 equiv.). The solution was subjected to a microwave-assisted reaction (CEM Discovery-SP microwave, 150 W, 250 psi, 413 K, 4×10 min reaction cycles) and then cooled to ambient temperature. The solution was filtered to remove insoluble particles and the solvent removed under reduced pressure to afford a pale brown amorphous solid (536 mg, 0.36 mmol, 72%). This intermediate was used directly without further purification for the preparation of catalyst **5**.

Synthesis of [Os(p-Cymene)(TsDPEN)] Complex 4

Complex **4** was prepared as previously reported.[8a] To a solution of non-tethered Os dimer **2** (51.4 mg, 0.065 mmol, 1 equiv.) and (*R*,*R*)-TsDPEN (51.3 mg, 0.14 mmol, 2.1 equiv.) in dichloromethane (10 mL) was added water (10 mL) and potassium hydroxide pellets (56.1 mg, 1 mol, 15 equiv.) with stirring for 10 min. The organic phase was diluted with dichloromethane (40 mL) and washed with water (2×50 mL), dried over magnesium sulphate, and concentrated to afford a dark red oil. The oil was recrystallized in dichloromethane/hexane to afford a red crystalline solid (68 mg, 0.10 mol, 75%). ^{1}H NMR (400 MHz, $CDCl_3$, 25 °C, TMS): δ = 7.41 (d, ArH, ^3J(H,H) = 7.6 Hz, 2H), 7.05–7.20 (m, ArH, 10H), 6.82 (d, ArH, ^3J(H,H) = 8.0 Hz, 2H), 6.80 (*br* s, NH, 1H), 5.79 (d, Os–ArH, ^3J(H,H) = 5.6 Hz, 1H), 5.62 (d, Os–ArH, ^3J(H,H) = 5.6 Hz, 1H), 5.52 (d, Os–ArH, ^3J(H,H) = 5.6 Hz, 1H), 5.42 (d, Os–ArH, ^3J(H,H) = 5.6 Hz, 1H), 4.42 (s, $CHCHNH_2$,1H), 3.94 (d, TsNCH, ^3J(H,H) = 4.3 Hz, 1H), 2.45 (sept, $CH(CH_3)_2$, ^3J(H,H) = 6.9 Hz, 1H), 2.23 (s, CH_3, 3H), 2.22 (s, CH_3, 3H), 1.23 (d, $CH(CH_3)_2$), ^3J(H,H) = 6.9 Hz, 3H) 1.17 (d, $CH(CH_3)_2$, ^3J(H,H) = 6.9 Hz, 3H); ^{13}C NMR (100 MHz, $CDCl_3$, 25 °C, TMS) δ = 127.4, 127.0, 126.8, 126.0, 125.9, 125.9, 125.4, 81.7, 76.2, 72.4, 70.7, 70.0, 66.2, 22.5, 22.4, 20.2; UV/Vis: λ_{max} 260, 410 and 478 nm; HR-MS (ESI): *m/z* calculated for $C_{31}H_{35}N_2O_2OsS$ $[M+H]^+$: 691.2028. Found: 691.2031. Elemental analysis (calculated, found for $C_{31}H_{34}N_2O_2OsS$): C (54.05, 53.66), H (4.97, 4.88), N (4.07, 3.95).

Synthesis of Tethered Osmium Complex 5

To a solution of Os pre-tether dimer **3** (149 mg, 0.10 mmol, 0.5 equiv.) in dichloromethane (25 mL) was added water (25 mL) and potassium hydroxide pellets (112 mg, 1 mmol, 10 equiv.) with stirring for 10 min. The organic phase was washed with water (2×50 mL), then dried over magnesium sulphate and concentrated to afford a dark red oil. The oil was recrystallised in dichloromethane/hexane to afford a red semi-crystalline solid (106 mg, 0.16 mol, 79%). ^{1}H NMR (400 MHz, $CDCl_3$, 25 °C, TMS): δ = 6.85–7.51 (m, 14H, ArH), 6.01–6.09 (m, 1H, Os–ArH), 5.92–6.01 (m, 2H, Os–ArH), 5.81–5.89 (m, 1H, Os–ArH), 5.33–5.42 (m, 1H, Os–ArH), 4.43 (s, 1H, CH), 3.73 (s, 1H, CH), 2.41–2.59 (m, 2H, CH_2), 2.32 (s, 3H, CH_3), 2.19–2.29 (m, 2H, CH_2), 1.81–1.89 (m, 2H, CH_2); ^{13}C NMR (100 MHz, $CDCl_3$, 25 °C, TMS) δ = 146.4, 146.3, 141.5, 141.4, 140.5, 129.1, 128.4, 128.4, 128.3, 128.3, 128.3, 128.3, 127.9, 127.6, 127.4, 127.3, 127.1, 126.8, 126.5, 92.1, 88.3, 73.3, 70.2, 69.1, 65.4, 64.9, 59.6, 34.2, 30.2, 21.4; HR-MS (ESI): *m/z* calculated for $C_{30}H_{30}KN_2O_2OsS$ $[M+K]^+$: 713.1280. Found: 713.1278. HPLC Purity (254 nm): 98.3%.

Density Functional Theory Calculations

Initial input structures for tethered complex **5** were achieved by structural modification of crystallographic data for a similar 18e$^-$ Ru tethered complex (CCDC 913682) using GaussView 6.0.[20] Geometry optimization calculations were carried out in the gas phase using Gaussian 16, using the hybrid Perdew-Burke-Ernzerhof functional (PBE0) with the LanI2DZ (including effective core potential for Os) and 6-31 + G** (all other atoms) basis sets. Energy minima were confirmed by the lack of imaginary vibrational modes.

Transfer Hydrogenation of Acetophenone

Os complex **5** (1 mol. equiv.) was weighed into a round bottomed flask and placed under an inert atmosphere of nitrogen, to which was added 5 : 2 v/v formic acid/triethylamine azeotrope (0.5 mL) and d_6-benzene (100 μL) by syringe and the catalyst stirred at 310 K. After 5 min, 120 μL of the catalytic substrate, acetophenone (200 mol. equiv.) was added by syringe and the mixture transferred to a 5 mm NMR tube (t = 0 h). ^{1}H NMR spectra were recorded at 73 s intervals for 3 h at 310 ± 0.5 K using a Bruker AV-400 spectrometer. ^{1}H NMR data were processed using TopSpin 3.2 for Windows. Substrate conversion was determined by measuring the ratio of integrals of peaks from 2.25–2.65 ppm (substrate CH_3 singlet) and 4.55–5.00 ppm (product C*H*(OH) quartet), which in turn was converted to turnover number and turnover frequency, given the substrate : catalyst ratio (200 : 1). The experiment was carried

out in triplicate with mean and the associated standard deviations reported.

Extracellular Speciation Analysis

Briefly, 10 μM solutions of Os complex **5** were prepared in three biological matrixes (600 μM bovine albumin, foetal calf serum, or human serum; all containing 5% DMSO to aid solubility) and were incubated at 310 K for 24 h. After this time, samples were analysed using an optimised offline LC-ICP-MS methodology. Samples were diluted 10-fold with 50 mM Tris solution (pH 7.4) prior to analysis. The liquid chromatographic separation (LC) was achieved using an Agilent 1200 series HPLC fitted with a TSKgel Q-STAT strong anion exchange column (7 μm, 10 cm×4.6 mm i.d.) with a flow rate of 0.7 mL·min^{-1} and an injection volume of 100 μL. Buffer A: 50 mM Tris base, pH 7.4. Buffer B: 50 mM Tris base + 1 M ammonium acetate, pH 7.4. Gradient (linear): 0–3 min, 0% B; 3–9 min, 20% B; 9–13.5 min, 50% B; 13.5–16.5 min, 100% B; 16.5–22.5 min, 100% B; 22.5–27 min, 0% B; 27–30 min, 0% B (re-equilibration). Elemental data for ^{56}Fe (He-gas mode), ^{63}Cu (He-gas mode), ^{66}Zn (He-gas mode) and ^{189}Os (no-gas mode) were obtained offline using an Agilent 7900 series ICP-MS, with calibration standards prepared from 1000 mg·L^{-1} certified reference materials using 50 mM Tris solution (pH 7.4) as a diluent. Data were acquired and processed using MassHunter 4.4 (version C.01.04, build 544.8, Agilent Technologies, Inc.).

Antiproliferative Activity Determination

Initially, 5×10^3 cells per well were seeded in 96 well plates and incubated for 48 h (310 K). Solutions of test compounds were prepared in culture medium containing <5% DMSO (*v/v*) to aid solubility ("*Aqueous stability studies*" in the Supporting Information). Solution concentrations were determined as described below ("*Determination of Os concentrations*"). The supernatant was removed and replaced with medium containing six known concentrations of test compound (typically 0.1–100 μM, 200 μL per well) and cells were exposed for 24 h. After this time, the supernatant was removed by aspiration, cells were washed with DPBS and allowed 72 h recovery time in fresh medium (in the absence of test compound). Cells were fixed by addition of trichloroacetic acid (50 mM, 50 μL per well, 1 h, 277 K) and cell viability was determined using the SRB assay as previously described.[24] Experiments were carried out in triplicate as part of two independent experiments (duplicate of triplicate). Half-maximal inhibitory concentrations (IC_{50}) were determined relative to the untreated negative control, and standard deviations were calculated. Exemplar dose-response sigmoidal curve fits are found in the Supporting Information.

Determination of Os Concentrations

Stock solutions from antiproliferative activity determinations were analysed using a Perkin Elmer Optima 5300 DV Series Inductively Coupled Plasma Optical Emission Spectrophotometer (ICP-OES). Calibration standards for Os and Pt were freshly prepared in 3.6% v/v nitric acid supplemented with thiourea (10 mM) and ascorbic acid (50 mg·L^{-1}). Samples were diluted to within the calibration range (50–700 ppb), with the matrix of the calibration standards and calibration blanks adjusted by standard addition of sodium chloride (99.999% trace metal basis) to match that of the samples. Data were acquired and processed using WinLab32V3.4.1 for Windows.

Modulation of Antiproliferative Activity

In a modification of the antiproliferative activity determination protocol, MCF7, MCF7–TAMR-1, MCF10-A or MDA–MB-231 cells were treated with a fixed sub-lethal concentration (0.5×IC_{50}) of Os catalyst **5** in the presence of sodium formate or sodium acetate (0, 0.5, 1 or 2 mM) for 24 h. Sodium formate and sodium acetate were added independently of the Os catalyst but within 5 min. Cell viability was determined using the SRB assay as previously described. Cell survival was calculated relative to the formate-free (or acetate-free) cell population and standard deviations were calculated. Experiments were carried out in triplicate as part of two independent experiments (duplicate of triplicate analysis). Statistics were calculated using a two-tailed *t*-test assuming unequal sample variances (Welch's *t*-test).

Os Accumulation in Cancer Cells

Briefly, 4×10^6 MCF7 or MDA–MB-231 breast cancer cells were seeded in P100 plates using 10 mL of culture medium per plate and incubated for 24 h, after which time the supernatant media was removed and cells were treated with a fixed concentration (1×IC_{50}) of Os catalyst **5** for 24 h (310 K) without recovery time. After exposure, the Os-containing medium was removed by aspiration, cells were washed with DPBS and harvested using trypsin/EDTA. A cell count was performed for sample normalization. Cell pellets were obtained by centrifugation (1000 rpm, 5 min) which were re-suspended in DPBS (1 mL) prior to final centrifugation (1000 rpm, 5 min) to obtain pellets for chemical analysis. Cell pellets were obtained in triplicate (three biological experimental replicates). This experiment was repeated with the following modifications based on a previously reported methodology.[35a] *Untreated (negative control):* Cells were not treated with Os catalyst **5**. Cells were incubated for 24 h (310 K) prior to harvesting cell pellets. *Time-dependent Os accumulation:* Cells were treated with a fixed concentration (1×IC_{50}) of Os catalyst **5** for 3 h or 6 h (310 K) without recovery time. Cells were also treated with Os catalyst **5** for 24 h, after which time the cells were washed with DPBS and allowed a further 72 h recovery time in Os-free medium. *Temperature-dependent Os accumulation:* Cells were treated with a fixed concentration (1×IC_{50}) of Os catalyst **5** for 3 h or 6 h (277 K) without recovery time. *Involvement of Na^+/K^+ pump in Os accumulation:* Cells were treated with a fixed concentration (1×IC_{50}) of Os catalyst **5** for 24 h (310 K) without recovery time in the presence of a non-toxic concentration of ouabain octahydrate (0.2 mM). *Involvement of protein-mediated transport in Os accumulation:* Cells were treated with a fixed concentration (1×IC_{50}) of Os catalyst **5** for 24 h (310 K) without recovery time in the presence of a non-toxic concentration of amphotericin B (20 μM). *Involvement of caveolin-mediated endocytosis in Os accumulation:* Cells were treated with a fixed concentration (1×IC_{50}) of Os catalyst **5** for 24 h (310 K) without recovery time in the presence of a non-toxic concentration of β-methyl cyclodextrin (1 mM). *Involvement of the Ctr1 transporter in Os accumulation:* Cells were treated with a fixed concentration (1×IC_{50}) of Os catalyst **5** for 24 h (310 K) without recovery time in the presence of a non-toxic concentration of copper(II) chloride (0.2 mM). *Involvement of formate or acetate in Os accumulation:* Cells were treated with a fixed concentration (1×IC_{50}) of Os catalyst **5** for 24 h (310 K) without recovery time in the presence of a non-toxic concentration of sodium formate or sodium acetate (2 mM). *Involvement of P-gp in Os efflux:* Cells were treated with a fixed concentration (1×IC_{50}) of Os catalyst **5** for 24 h, after which time the cells were washed with DPBS and allowed a further 72 h recovery time in Os-free medium containing 20 μM verapamil hydrochloride, a selective inhibitor of the p-glycoprotein (P-gp) efflux transporter. Cell pellets were subjected to acidic digestion (200 μL of 72% ultra-

pure nitric acid, 353 K, overnight) prior to dilution to a working acid concentration of 3.6% v/v using Type I Milli-Q water supplemented with thiourea (10 mM) and ascorbic acid (50 $mg \cdot L^{-1}$) to stabilize Os in nitric acid solution. Samples were analysed using an Agilent Technologies 7900 series ICP-MS, operated in He-gas mode (^{189}Os, ^{66}Zn, ^{63}Cu) and H_2-gas mode (^{56}Fe) with an internal standard inline infusion of 50 ppb ^{166}Er. External calibrants for Os, Zn, Cu and Fe were prepared from certified reference materials (1000 $mg \cdot L^{-1}$) ranging from 0.1–1000 $\mu g \cdot L^{-1}$ in 3.6% v/v HNO_3 supplemented with thiourea (10 mM) and ascorbic acid (50 $mg \cdot L^{-1}$). ICP-MS data were acquired as instrumental (technical) triplicates for each experimental replicate. Data were normalised by cell count and reported as the mean value (femtograms of osmium per cell) with the associated standard deviation (N = 3).

Fluorescence Microscopy

Briefly, 1×10^4 MCF7 breast cancer cells were seeded in a 24 well plate using 0.5 mL per well, and incubated for 48 h at 310 K. After this time, cells were treated with test compounds ($1 \times IC_{50}$, 0.5 mL per well) for 24 h (or cell culture medium only for the negative untreated control). Positive control wells were treated with 50 μM Antimycin A for 30 min in the dark prior to staining.[39b] All cells were washed with DPBS (1×0.5 mL) and stained using 2′,7′-dichlorodihydrofluorescein diacetate (H_2–DCFDA, 10 $\mu g \cdot mL^{-1}$) for 20 min in the dark at 310 K. Cells were washed using DPBS (2×0.5 mL) to remove excess dye and imaged using an EVOS FL fluorescence microscope fitted with a GFP filter cube ($\lambda_{Ex/Em}$ = 470/510 nm, exposure time 0.5 sec, intensity 50%).

Acute in Vivo Zebrafish Embryo Toxicity

In vivo experiments were carried out using Singapore wild-type zebrafish embryos under project AWERB.85/21-22. The University of Warwick is a member of the Institute of Animal Technology and the Laboratory Animal Science Association. Zebrafish were maintained in accordance with ASPA 1986 by Mr. Ian Bagley, using 3.5 L tanks (checked daily for water quality) in a 14 h light cycle, and provided with food (live and powder) four times a day during the week and twice a day during weekends. Fish were mated in breeding tanks fitted with a divider. Two mating pairs were used per breeding tank, and the divider was removed at dawn. Acute *in vivo* toxicities were determined according to OECD Test 236: "Fish Embryo Acute Toxicity (FET)" and as previously reported.[41] Freshly harvested embryos were collected at dawn and fertilized embryos were seeded at a density of 2–3 embryos per well in 24 well plates. Serial dilutions of complex **5** and cisplatin were prepared in egg water (typically 0.01–100 μM, 1 mL per well, 20 wells per test concentration) and embryos were exposed for 96 h at 301 K. The experiment included two positive (2,3-dichloroaniline) and two negative control wells (untreated embryos, egg water only) on each 24-well plate. Embryo viability was determined according to four criteria – if any (or multiple) attributes were observed, the embryo was considered non-viable – (1) lack of heartbeat, (2) coagulation of fertilized egg, (3) lack of somite formation, (4) lack of tail-bud detachment from the yolk sac. A sigmoidal dose-response curve was obtained (embryo survival as a function of concentration) and fitted using GraphPad Prism 10. This experiment was carried out as part of two independent biological experiments, each with 20 replicates per test concentration. Data were reported as the average of the two independent experiments, with an associated standard deviation. Dose-response sigmoidal curve fits can be found in the Supporting Information.

Supporting Information

The Supporting Information is available free of charge online. Computational data (density functional theory calculations) are available upon reasonable request to the authors. The authors have cited additional references within the Supporting Information.[8a,19,21,24,35a,39b,41]

Acknowledgements

We thank the Royal Society of Chemistry (grant no. E22-1637945680) and the University of Birmingham for support. PJS research is supported by Anglo American Platinum and the EPSRC (grant no. EP/P030572/1). We thank the University of Warwick Analytical Science CDT and GoldenKeys High-Tech Materials Co. Ltd for a PhD CASE studentship for OWLC.

Conflict of Interests

The authors declare no conflict of interest.

Data Availability Statement

The data that support the findings of this study are available in the supplementary material of this article.

Keywords: osmium · *in-cell* catalysis · cancer · transfer hydrogenation · redox

[1] M. Hoppert, in *Encyclopedia of Geobiology* (Eds.: J. Reitner, V. Thiel), Springer Netherlands, Dordrecht, **2011**, pp. 558–563.
[2] a) J. J. Soldevila-Barreda, P. J. Sadler, *Curr. Opin. Chem. Biol.* **2015**, *25*, 172–183; b) Z. Yu, J. A. Cowan, *Chem. Eur. J.* **2017**, *23*, 14113–14127; c) E. J. Anthony, E. M. Bolitho, H. E. Bridgewater, O. W. L. Carter, J. M. Donnelly, C. Imberti, E. C. Lant, F. Lermyte, R. J. Needham, M. Palau, P. J. Sadler, H. Shi, F. X. Wang, W. Y. Zhang, Z. Zhang, *Chem. Sci.* **2020**, *11*, 12888–12917; d) J. J. Soldevila-Barreda, N. Metzler-Nolte, *Chem. Rev.* **2019**, *119*, 829–869; e) S. Alonso-de Castro, A. Terenzi, J. Gurruchaga-Pereda, L. Salassa, *Chem. Eur. J.* **2019**, *25*, 6651–6660.
[3] a) J. T. Weiss, J. C. Dawson, K. G. Macleod, W. Rybski, C. Fraser, C. Torres-Sánchez, E. E. Patton, M. Bradley, N. O. Carragher, A. Unciti-Broceta, *Nat. Commun.* **2014**, *5*, 3277; b) J. T. Weiss, J. C. Dawson, C. Fraser, W. Rybski, C. Torres-Sánchez, M. Bradley, E. E. Patton, N. O. Carragher, A. Unciti-Broceta, *J. Med. Chem.* **2014**, *57*, 5395–5404.
[4] T. Völker, F. Dempwolff, P. L. Graumann, E. Meggers, *Angew. Chem. Int. Ed.* **2014**, *53*, 10536–10540.
[5] a) J. J. Soldevila-Barreda, K. B. Fawibe, M. Azmanova, L. Rafols, A. Pitto-Barry, U. B. Eke, N. P. E. Barry, *Molecules* **2020**, *25*(19), 4540, DOI: 10.3390/molecules25194540; b) W.-Y. Zhang, H. E. Bridgewater, S. Banerjee, J. J. Soldevila-Barreda, G. J. Clarkson, H. Shi, C. Imberti, P. J. Sadler, *Eur. J. Inorg. Chem.* **2020**, *2020*, 1052–1060; c) R. A. Sarfraz, T. G. Kazi, S. Iqbal, H. I. Afridi, M. K. Jamali, N. Jalbani, M. B. Arain, *Appl. Organomet. Chem.* **2008**, *22*, 187–192.
[6] a) D. Kong, M. Tian, L. Guo, X. Liu, S. Zhang, Y. Song, X. Meng, S. Wu, L. Zhang, Z. Liu, *J. Biol. Inorg. Chem.* **2018**, *23*, 819–832; b) S. J. Dougan, A. Habtemariam, S. E. McHale, S. Parsons, P. J. Sadler, *Proc. Natl. Acad. Sci. USA* **2008**, *105*, 11628–11633; c) W. Y. Zhang, S. Banerjee, G. M. Hughes, H. E. Bridgewater, J. I. Song, B. G. Breeze, G. J. Clarkson, J. P. C. Coverdale, C. Sanchez-Cano, F. Ponte, E. Sicilia, P. J. Sadler, *Chem. Sci.* **2020**, *11*, 5466–5480.

[7] a) J. J. Soldevila-Barreda, I. Romero-Canelón, A. Habtemariam, P. J. Sadler, *Nat. Commun.* **2015**, *6*, 6582; b) R. Kushwaha, A. Kumar, S. Saha, S. Bajpai, A. K. Yadav, S. Banerjee, *Chem. Commun.* **2022**, *58*, 4825–4836.
[8] a) J. P. C. Coverdale, C. Sanchez-Cano, G. J. Clarkson, R. Soni, M. Wills, P. J. Sadler, *Chem. Eur. J.* **2015**, *21*, 8043–8046; b) E. M. Bolitho, N. G. Worby, J. P. C. Coverdale, J. A. Wolny, V. Schünemann, P. J. Sadler, *Organometallics* **2021**, *40*, 3012–3023.
[9] J. P. C. Coverdale, I. Romero-Canelón, C. Sanchez-Cano, G. J. Clarkson, A. Habtemariam, M. Wills, P. J. Sadler, *Nat. Chem.* **2018**, *10*, 347–354.
[10] E. M. Bolitho, J. P. C. Coverdale, H. E. Bridgewater, G. J. Clarkson, P. D. Quinn, C. Sanchez-Cano, P. J. Sadler, *Angew. Chem. Int. Ed.* **2021**, *60*, 6462–6472.
[11] A. M. R. Hall, P. Dong, A. Codina, J. P. Lowe, U. Hintermair, *ACS Catal.* **2019**, *9*, 2079–2090.
[12] a) H. J. Davis, T. R. Ward, *ACS Cent. Sci.* **2019**, *5*, 1120–1136; b) F. Schwizer, Y. Okamoto, T. Heinisch, Y. Gu, M. M. Pellizzoni, V. Lebrun, R. Reuter, V. Köhler, J. C. Lewis, T. R. Ward, *Chem. Rev.* **2018**, *118*, 142–231.
[13] a) N. Soliman, G. Gasser, C. M. Thomas, *Adv. Mater.* **2020**, *32*, 2003294; b) S. R. Alves, A. Colquhoun, X. Y. Wu, D. de Oliveira Silva, *J. Inorg. Biochem.* **2020**, *205*, 110984; c) J. Karges, D. Díaz-García, S. Prashar, S. Gómez-Ruiz, G. Gasser, *ACS Appl. Bio Mater.* **2021**, *4*, 4394–4405.
[14] a) F. Martínez-Peña, S. Infante-Tadeo, A. Habtemariam, A. M. Pizarro, *Inorg. Chem.* **2018**, *57*, 5657–5668; b) A. C. Carrasco, V. Rodríguez-Fanjul, A. M. Pizarro, *Inorg. Chem.* **2020**, *59*, 16454–16466; c) S. Infante-Tadeo, V. Rodriguez, A. Habtemariam, A. M. Pizarro, *Chem. Sci.* **2021**, *12*, 9287–9297.
[15] a) D. J. Morris, A. M. Hayes, M. Wills, *J. Org. Chem.* **2006**, *71*, 7035–7044; b) J. Hannedouche, G. J. Clarkson, M. Wills, *J. Am. Chem. Soc.* **2004**, *126*, 986–987.
[16] a) R. Soni, T. H. Hall, B. P. Mitchell, M. R. Owen, M. Wills, *J. Org. Chem.* **2015**, *80*, 6784–6793; b) F. Chen, I. Romero-Canelón, J. J. Soldevila-Barreda, J. I. Song, J. P. C. Coverdale, G. J. Clarkson, J. Kasparkova, A. Habtemariam, M. Wills, V. Brabec, P. J. Sadler, *Organometallics* **2018**, *37*, 1555–1566.
[17] R. Soni, K. E. Jolley, G. J. Clarkson, M. Wills, *Org. Lett.* **2013**, *15*, 5110–5113.
[18] K. E. Jolley, A. Zanotti-Gerosa, F. Hancock, A. Dyke, D. M. Grainger, J. A. Medlock, H. G. Nedden, J. J. M. Le Paih, S. J. Roseblade, A. Seger, V. Sivakumar, I. Prokes, D. J. Morris, M. Wills, *Adv. Synth. Catal.* **2012**, *354*, 2545–2555.
[19] J. Tönnemann, J. Risse, Z. Grote, R. Scopelliti, K. Severin, *Eur. J. Inorg. Chem.* **2013**, *2013*, 4558–4562.
[20] a) G. W. T. M. J. Frisch, H. B. Schlegel, G. E. Scuseria, M. A. Robb, J. R. Cheeseman, G. Scalmani, V. Barone, G. A. Petersson, H. Nakatsuji, X. Li, M. Caricato, A. V. Marenich, J. Bloino, B. G. Janesko, R. Gomperts, B. Mennucci, H. P. Hratchian, J. V. Ortiz, A. F. Izmaylov, J. L. Sonnenberg, D. Williams-Young, F. Ding, F. Lipparini, F. Egidi, J. Goings, B. Peng, A. Petrone, T. Henderson, D. Ranasinghe, V. G. Zakrzewski, J. Gao, N. Rega, G. Zheng, W. Liang, M. Hada, M. Ehara, K. Toyota, R. Fukuda, J. Hasegawa, M. Ishida, T. Nakajima, Y. Honda, O. Kitao, H. Nakai, T. Vreven, K. Throssell, J. A. Montgomery, Jr., J. E. Peralta, F. Ogliaro, M. J. Bearpark, J. J. Heyd, E. N. Brothers, K. N. Kudin, V. N. Staroverov, T. A. Keith, R. Kobayashi, J. Normand, K. Raghavachari, A. P. Rendell, J. C. Burant, S. S. Iyengar, J. Tomasi, M. Cossi, J. M. Millam, M. Klene, C. Adamo, R. Cammi, J. W. Ochterski, R. L. Martin, K. Morokuma, O. Farkas, J. B. Foresman, D. J. Fox, Gaussian 16, Revision C.01, Gaussian, Inc., Wallingford CT, **2016**; b) T. A. K. R. Dennington, J. M. Millam, GaussView, Version 6, Semichem Inc, Shawnee Mission, KS, **2016**.
[21] A. M. Hayes, D. J. Morris, G. J. Clarkson, M. Wills, *J. Am. Chem. Soc.* **2005**, *127*, 7318–7319.
[22] R. Soni, F. K. Cheung, G. C. Clarkson, J. E. D. Martins, M. A. Graham, M. Wills, *Org. Biomol. Chem.* **2011**, *9*, 3290–3294.
[23] X. Dai, H. Cheng, Z. Bai, J. Li, *J. Cancer* **2017**, *8*, 3131–3141.
[24] V. Vichai, K. Kirtikara, *Nat. Protoc.* **2006**, *1*, 1112–1116.
[25] S.-C. Chien, C.-Y. Chen, C.-F. Lin, H.-I. Yeh, *Biomark. Res.* **2017**, *5*, 31.
[26] a) V. Novohradský, A. Bergamo, M. Cocchietto, J. Zajac, V. Brabec, G. Mestroni, G. Sava, *Dalton Trans.* **2015**, *44*, 1905–1913; b) O. Dömötör, C. G. Hartinger, A. K. Bytzek, T. Kiss, B. K. Keppler, E. A. Enyedy, *J. Biol. Inorg. Chem.* **2013**, *18*, 9–17; c) J. Lu, A. J. Stewart, P. J. Sadler, T. J. Pinheiro, C. A. Blindauer, *Biochem. Soc. Trans.* **2008**, *36*, 1317–1321.
[27] J.-J. Qin, L. Yan, J. Zhang, W.-D. Zhang, *J. Exp. Clin. Cancer Res.* **2019**, *38*, 195.
[28] W. Feng, Y. He, J. Xu, H. Zhang, Y. Si, J. Xu, S. Li, *Anticancer Drugs* **2022**, *33*(1), e52–e60.
[29] L. Bian, P. Yu, J. Wen, N. Li, W. Huang, X. Xie, F. Ye, *NPJ Breast Cancer* **2021**, *7*, 157.
[30] F. Poggio, M. Bruzzone, M. Ceppi, N. F. Pondé, G. La Valle, L. Del Mastro, E. de Azambuja, M. Lambertini, *Ann. Oncol.* **2018**, *29*, 1497–1508.
[31] a) S. Zhao, J. Huang, J. Ye, *J. Exp. Clin. Cancer Res.* **2015**, *34*, 80; b) P. M. Eimon, A. L. Rubinstein, *Expert Opin. Drug Metab. Toxicol.* **2009**, *5*, 393–401.
[32] C. A. MacRae, R. T. Peterson, *Nat. Rev. Drug Discovery* **2015**, *14*, 721–731.
[33] a) G. J. Lieschke, P. D. Currie, *Nat. Rev. Genet.* **2007**, *8*, 353–367; b) W. B. Barbazuk, I. Korf, C. Kadavi, J. Heyen, S. Tate, E. Wun, J. A. Bedell, J. D. McPherson, S. L. Johnson, *Genome Res.* **2000**, *10*, 1351–1358.
[34] K. Howe, M. D. Clark, C. F. Torroja, J. Torrance, C. Berthelot, M. Muffato, J. E. Collins, S. Humphray, K. McLaren, L. Matthews, S. McLaren, I. Sealy, M. Caccamo, C. Churcher, C. Scott, J. C. Barrett, R. Koch, G.-J. Rauch, S. White, W. Chow, B. Kilian, L. T. Quintais, J. A. Guerra-Assunção, Y. Zhou, Y. Gu, J. Yen, J.-H. Vogel, T. Eyre, S. Redmond, R. Banerjee, J. Chi, B. Fu, E. Langley, S. F. Maguire, G. K. Laird, D. Lloyd, E. Kenyon, S. Donaldson, H. Sehra, J. Almeida-King, J. Loveland, S. Trevanion, M. Jones, M. Quail, D. Willey, A. Hunt, J. Burton, S. Sims, K. McLay, B. Plumb, J. Davis, C. Clee, K. Oliver, R. Clark, C. Riddle, D. Elliott, G. Threadgold, G. Harden, D. Ware, S. Begum, B. Mortimore, G. Kerry, P. Heath, B. Phillimore, A. Tracey, N. Corby, M. Dunn, C. Johnson, J. Wood, S. Clark, S. Pelan, G. Griffiths, M. Smith, R. Glithero, P. Howden, N. Barker, C. Lloyd, C. Stevens, J. Harley, K. Holt, G. Panagiotidis, J. Lovell, H. Beasley, C. Henderson, D. Gordon, K. Auger, D. Wright, J. Collins, C. Raisen, L. Dyer, K. Leung, L. Robertson, K. Ambridge, D. Leongamornlert, S. McGuire, R. Gilderthorp, C. Griffiths, D. Manthravadi, S. Nichol, G. Barker, S. Whitehead, M. Kay, J. Brown, C. Murnane, E. Gray, M. Humphries, N. Sycamore, D. Barker, D. Saunders, J. Wallis, A. Babbage, S. Hammond, M. Mashreghi-Mohammadi, L. Barr, S. Martin, P. Wray, A. Ellington, N. Matthews, M. Ellwood, R. Woodmansey, G. Clark, J. D. Cooper, A. Tromans, D. Grafham, C. Skuce, R. Pandian, R. Andrews, E. Harrison, A. Kimberley, J. Garnett, N. Fosker, R. Hall, P. Garner, D. Kelly, C. Bird, S. Palmer, I. Gehring, A. Berger, C. M. Dooley, Z. Ersan-Ürün, C. Eser, H. Geiger, M. Geisler, L. Karotki, A. Kirn, J. Konantz, M. Konantz, M. Oberländer, S. Rudolph-Geiger, M. Teucke, C. Lanz, G. Raddatz, K. Osoegawa, B. Zhu, A. Rapp, S. Widaa, C. Langford, F. Yang, S. C. Schuster, N. P. Carter, J. Harrow, Z. Ning, J. Herrero, S. M. J. Searle, A. Enright, R. Geisler, R. H. A. Plasterk, C. Lee, M. Westerfield, P. J. de Jong, L. I. Zon, J. H. Postlethwait, C. Nüsslein-Volhard, T. J. P. Hubbard, H. R. Crollius, J. Rogers, D. L. Stemple, *Nature* **2013**, *496*, 498–503.
[35] a) I. Romero-Canelón, A. M. Pizarro, A. Habtemariam, P. J. Sadler, *Metallomics* **2012**, *4*, 1271–1279; b) L. Chen, H. Wang, X. Li, C. Nie, T. Liang, F. Xie, K. Liu, X. Peng, J. Xie, *RSC Adv.* **2018**, *8*, 35246–35256.
[36] A. Ballesta, F. Billy, J. P. C. Coverdale, J. I. Song, C. Sanchez-Cano, I. Romero-Canelón, P. J. Sadler, *Metallomics* **2019**, *11*, 1648–1656.
[37] M. A. Summers, J. L. Moore, J. W. McAuley, *Ann. Pharmacother.* **2004**, *38*, 1631–1634.
[38] a) M. M. González-Ballesteros, C. Mejía, L. Ruiz-Azuara, *FEBS Open Bio* **2022**, *12*, 880–899; b) U. Jungwirth, C. R. Kowol, B. K. Keppler, C. G. Hartinger, W. Berger, P. Heffeter, *Antioxid. Redox Signaling* **2011**, *15*, 1085–1127; c) X. Li, Y. Wang, M. Li, H. Wang, X. Dong, *Molecules* **2021**, *27*(1), 148, https://doi.org/10.3390/molecules27010148.
[39] a) E. Eruslanov, S. Kusmartsev, in *Advanced Protocols in Oxidative Stress II* (Ed.: D. Armstrong), Humana Press, Totowa, NJ, **2010**, pp. 57–72; b) A. Wojtala, M. Bonora, D. Malinska, P. Pinton, J. Duszynski, M. R. Wieckowski, *Methods Enzymol.* **2014**, *542*, 243–262.
[40] W. H. Park, Y. W. Han, S. H. Kim, S. Z. Kim, *J. Cell. Biochem.* **2007**, *102*, 98–109.
[41] J. P. C. Coverdale, H. E. Bridgewater, J. I. Song, N. A. Smith, N. P. E. Barry, I. Bagley, P. J. Sadler, I. Romero-Canelón, *J. Med. Chem.* **2018**, *61*, 9246–9255.

Manuscript received: April 23, 2024
Revised manuscript received: May 23, 2024
Accepted manuscript online: May 24, 2024
Version of record online: July 9, 2024